UNIVERSIDAD POLITECNICA DE VALENCIA

DEPARTAMENTO DE COMUNICACIONES

Máster Universitario en Tecnologías, Sistemas y Redes de Comunicaciones

Characterization of a Photonic Generation System of G-band signals

Author: Guillem Peris Cuesta

Director: Borja Vidal Rodríguez

Starting Date: 6/4/2019

Workplace: Nanophotonics Technology Center

Objectives – The objective of this work is the characterization of a photonic-assisted transmitter in the G-band for wireless backhauling. This study will contribute to assess the potential performance of this approach and to identify the critical design limitations. This work has been carried out in the framework of EU H2020 project ULTRAWAVE.

Methodology – The project has been based on a classical methodology: review of the related theoretical background and the state of the art, theoretical study of the system, simulation and experimental validation. This process has been iterated to refine both theoretical and simulation models.

Theoretical development – A theoretical model to assess the performance of several aspects of the photonic transmitter has been developed. It has been implemented in MATLAB to identify critical parameters of the system. For data transmission, VPIphotonics software has been used.

Lab work and prototype development – All the activity performed during this Master Thesis has taken place at the Nanophotonics Technology Center of UPV, specifically in the "Optical Signal Processing and THz Photonics" group. Nearly all the components used have been purchased after previous theoretical estimations of the capabilities needed to build the prototype.

Results – The main result of the TFM is the design and analysis of the architecture for the photonic transmitter to be used in the EU project ULTRAWAVE. Some conclusions of this analysis are: a laser between 13-16 dBm is preferable for the system, 25 dBm of RF yields nearly the best response for two cascaded phase modulators, better ways to generate a wider comb need to be reviewed. Different optical paths and different optical delay limit final performance and care need to be paid to optimize this parameter. Linearity is characterized by 90 dB $\cdot$ Hz$^{2/3}$ of SFDR, around 30 dB of CNR are expected and a trade-off between number of channels, data rate and channel spacing needs to be settled. Simulations are provided for a four channel transmission, each of them with 2 Gbps of QPSK modulation and spacing of 4 GHz.

Future work– There are several lines where future work can be done. It would be worth devoting research efforts to investigate more efficient ways of generating harmonics away from the central wavelength since it strongly affects CNR. Other areas needing further work are the compensation of fiber length impact, linearization techniques such as low-bias or IMD3 compensation and practical data transmission.

Publications – Part of the results of this TFM have been included in Deliverable D5.2 of EU H2020 project ULTRAWAVE which is focused on the G-band Photonic Transmitter.

Abstract – Data traffic keeps raising in a way that current technology will not be able to hold with several bottlenecks ahead. G-band signals have gained attention in previous years because the unprecedented amount of available bandwidth to deliver fast and

simple ”fiber-on-air” backhaul enabling mobile architectures based on small cell densification to allow high bitrates. Photonic generation systems are well suited to provide wide bandwidth and compatibility with core optical network technology. This work focuses on the characterization of a photonic transmitter in the G-band. It is carried out in the framework of EU H2020 project ULTRAWAVE. After evaluation of possible architectures, external modulation of a CW laser is chosen and analogical characterization is performed where is determined that 25 dBm of RF power is needed. With this value around 30 dB of CNR is expected to be achieved and a SFDR of 90 $dB \cdot Hz^{2/3}$. Phase noise has been also measured. Regarding digital characterization, different simulations using *VPIphotonics* software have been performed, where it can be seen that 13-16 dBm of optical power is a good operation point. Critical parameters such as fiber length have been identified in the designing stage where 5 km can lead to 10% loss of EVM because of the singularity of this system, so pre-compensation will be mandatory in future work. Finally, it is demonstrated that an agreement between number of channels, data rate and channel spacing needs to be established, being in this case four channels, each with 2 Gbps and 4 GHz of spacing.

Author: Guillem Peris Cuesta, email: guipecue@teleco.upv.es
Director : Borja Vidal Rodríguez email: bvidal@dcom.upv.es
Delivery date: 9-9-19

Contents

1 Introduction

1.1 Microwave Photonics

Microwave Photonics (MWP) is the application of optical devices for the generation and processing of microwave signals [1]. This topic has attracted a lot of attention in recent decades, especially for signals in the upper bands, such as the millimeter and sub-THz regions [2]. Photonics offers an alternative path that allow to implement tasks that are very complex in all-electrical systems or even impossible. Moreover, advantages of optical fiber respect to electrical cables such as lower size, immunity to electromagnetic interference, ultra low losses, lower cost, lower weight or unprecedented data transfer capacity turned out to be key factors in the development of this technology.

A basic MWP system, also known as radio-over-fiber link, consists of an electrical signal to be transmitted or processed which is modulated onto a light beam by means of external or direct modulation. In its simplest form, this signal is transmitted over optical fiber and converted again into the electrical domain using a photodetector (as shown in Figure 1).

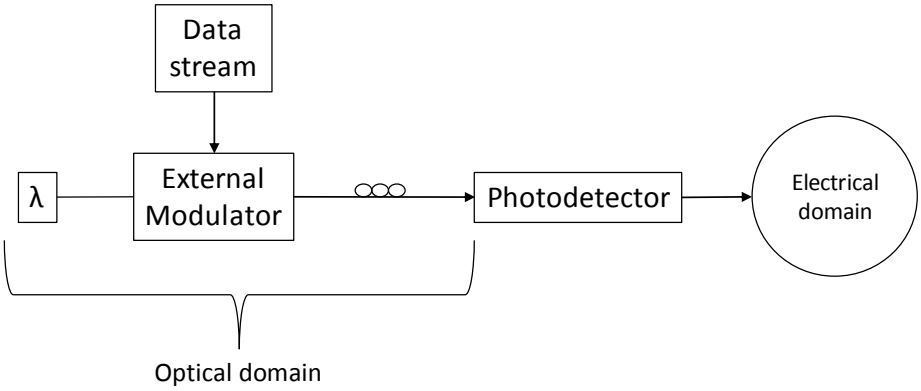

Figure 1: Typical example of a Microwave Photonics system. Electrical data stream is transmitted through optical domain and is converted into electrical signal again when photodetecting.

From the first experiments carried out in late 70's until nowadays, the applications of microwave photonics have widened. Some examples are: radio-over-fiber links for cellular, wireless and satellite applications (e.g. [3], [4]), optical beamforming to control large antennas arrays while keeping wide bandwidth (e.g. [5]), RF filters [6], sensing [7], and photonic-assisted microwave measurement [8], just to cite the most researched. One of the applications that most attention has attracted is photonic-assisted generation of high frequency signals, in particular in the millimeter and submillimeter bands, [2], [9]. This is the main topic of this work, the photonic generation of G-band (110 to 300 GHz) signals.

1.2 Traffic growth

Data traffic keeps increasing exponentially for multiple reasons. In the last years the main drivers of this rising demand have been: Internet of Things (IoT), online gaming, ultra high definition VOD, cloud computing, etc. In general, society is more connected, demands faster quality communications and lower latency, thus, higher bandwidth is required to meet this goals. According to Cisco systems, mobile data traffic increased 70% in 2014 and the IMT-2020 Promotion Group estimated that it will grow over 200 times from 2010 to 2020 and 20,000 times from 2010 to 2030. This sustained growth imposes a huge challenge to present wireless and core technologies which need to be scaled accordingly. One of these bottlenecks is in the backhaul for cellular networks. Most low frequency bands of the microwave region are crowded with many regulated wireless services. Thus, to provide high bitrate services, new frequency bands are needed. If fiber-like wireless bitrates are needed, bands in the millimeter and submillimeter-wave bands have a promising potential to avoid future bottlenecks in backhauling and enable future commercial communications such as 5G-NR and future 6G [10].

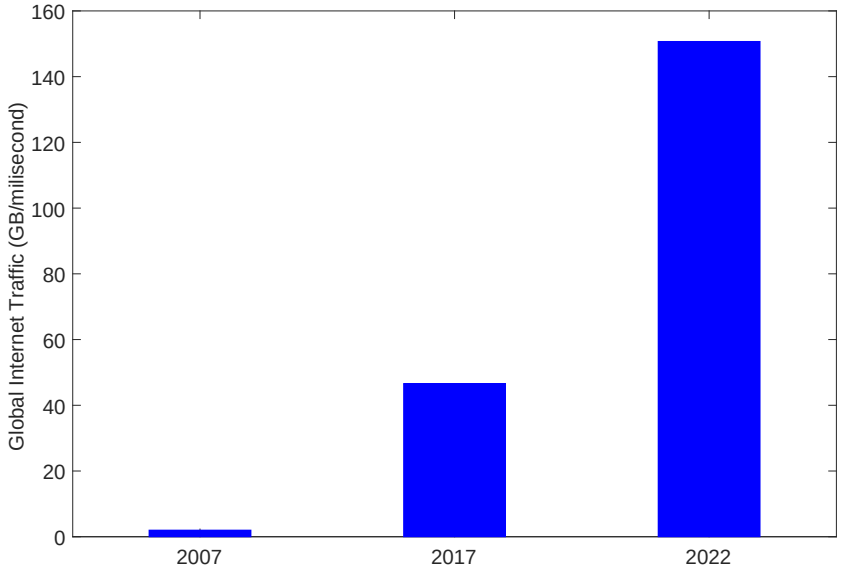

Figure 2: Global internet traffic growth prediction. Data gathered from Cisco Visual Networking Index 2018.

Among these unregulated bands in the upper millimeter-wave region, the G-band has several appealing features: it hosts a bandwidth of tens of GHz available, rain loss is relatively moderate and, for the moment, it is unregulated.

Given these features, the G-band appears as an attractive alternative to allocate many future high-demanding services as mentioned in [11]. Among these, cellular backhauling is particularly appealing given the strong pressure to cellular networks. Since building electrical oscillators at these frequencies with good performance is not easy, photonic generation systems are being studied. This alternative approach has been enabled by the

development of the uni-travelling-carrier photodiode (UTC-PD) by NTT researchers in the late 90s as an efficient photo-mixer at hundreds of GHz.

1.3 Photonic generation of microwave signals

One might think that heterodyning two free-running lasers would be the most straightforward way to generate signals at sub-THz band but given the free-running nature of the sources, the generated signal is not stable in frequency. Besides, since their phase noises are decorrelated post signal processing is required, resulting in more complex setups [12]. Using a coherent optical source solves the problem and several solutions have been proposed as comb generators, being an active research field during last decades. A brief summary of the main techniques for implementing coherent optical sources for photonic microwave generation is presented in the next sections, further information can be found in the literature, for example, [13].

1.3.1 Optical Injection Locking

Optical injection locking consists of one master laser that is directly frequency modulated, thus generating multiple sidebands. Then light is split and inserted into two different slave lasers whose frequencies of emission are very close to two master laser sidebands. Thus, phase locking (phase correlation) is achieved between tones that are combined and mixed at the photodetector, generating an electrical signal whose frequency is selected by means of slave lasers. An example can be seen in Figure 3.

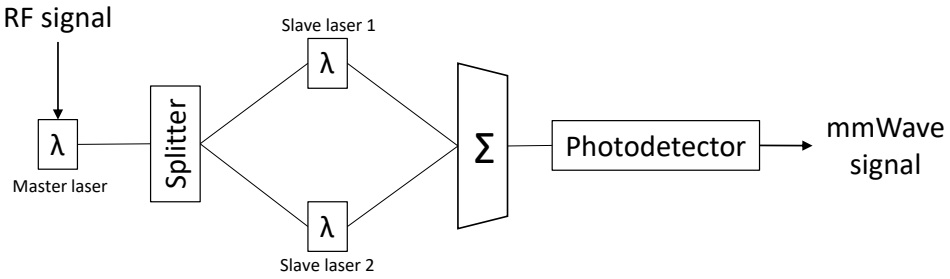

Figure 3: Optical injection locking setup.

1.3.2 Optical Phase Lock Loop

Another technique to obtain phase coherence between two optical tones is optical phase lock loops. In this case, two free-running lasers are beaten at a photodetector, generating an electrical signal that is compared with an RF reference. The phase comparison is fed into a loop filter that can control the phase of one laser in order to minimize the phase shift between them, thus locking the phase of the beat note to the RF reference. A typical setup is presented in Figure 4.

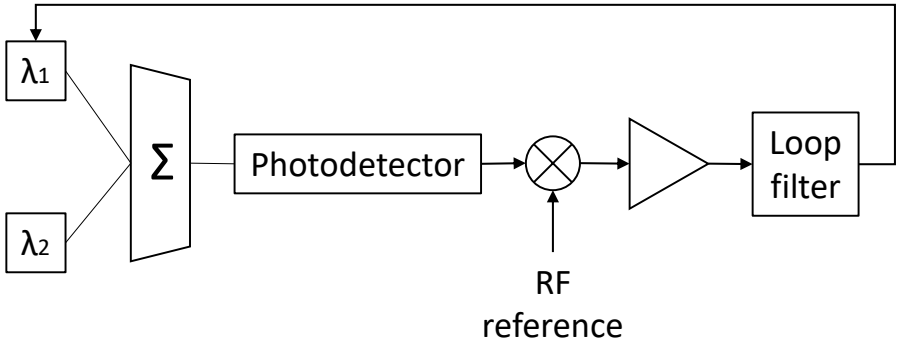

Figure 4: Optical phase lock loop example.

1.3.3 Optical Injection Phase Locking

The two above-mentioned techniques can be combined, in what is known as optical injection phase locking to further enhance phase noise. Figure 5 shows a case where a master laser is divided into two channels. One of them is externally modulated and the desired sideband is inserted into a slave laser for injection locking. Next the other channel and the locked one are mixed at the photodetector, generating an electrical signal. This tone is compared to a microwave reference and the optical phase fluctuations at the output of the slave laser are further reduced by a phase lock loop.

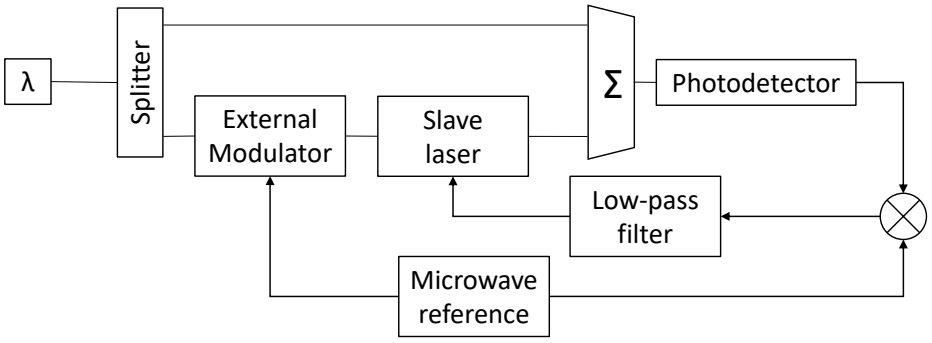

Figure 5: Optical injection phase locking system.

1.3.4 External Modulation

Coherent optical sources can also be generated using a single external modulator. In figure 6 it can be seen a generic system where one light beam is modulated by means of an RF signal that feeds the modulator. Multiple sidebands are thus generated with correlated phases. Regarding different types of modulators, Mach-Zehnder allows more flexibility depending on the polarization point for generating only even or only odd harmonics

whereas phase modulators generate all the harmonics and are less complex since they need no bias control.

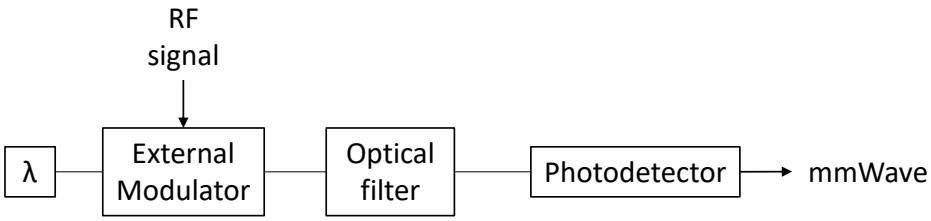

Figure 6: Optical coherent source using external modulation.

1.3.5 Dual-Wavelength Laser

Coherence can also be accomplished with a dual-wavelength laser with a wavelength spacing given by the desired frequency. No phase locking is carried out, however both light sources are generated at the same cavity and phase quality outperforms two free-running lasers, plus there is no need for a loop circuit or external device.

1.4 State of art of sub-THz data transmission

Finally, after all different techniques are presented, a review of the latest sub-THz generation systems is done. Figures 7 and 8 shows a summary of the state-of-the-art solutions to generate sub-THz signals, including both all-electrical and optoelectronical systems.

Combining both, in general, higher data rates and better *capacity x distance* parameters have been demonstrated in the sub-THz bands using optoelectronics solutions. In order to further investigate the potential of optoelectronics for wireless backhauling, EU H2020 ULTRAWAVE project has put together a set of researchers of different countries to improve the previous figure of merit mentioned by combining different technologies.

1.5 EU H2020 project ULTRAWAVE

ULTRAWAVE is a project that is aimed at developing a high capacity backhaul cell densification for 5G and future 6G by taking profit of bands beyond 100 GHz. This is going to serve more than 100 Gbps per square kilometer using a Point to Point G-band and Point to Multi point D-band (141-174.8 GHz) links.

Figure 9 gives an overview of the ULTRAWAVE's link proposal. It is shown how G-band PtP link is used to communicate base stations separated 600 meters away and D-band PtMp link delivers communications to numerous sectors/cells where users are served until 500 meters away. Knowing that these frequencies and distances cause enormous free-space losses, a new high-frequency amplifier is mandatory to overcome it, which is developed in the framework of this project, namely a new Traveling Wave Tube (TWT).

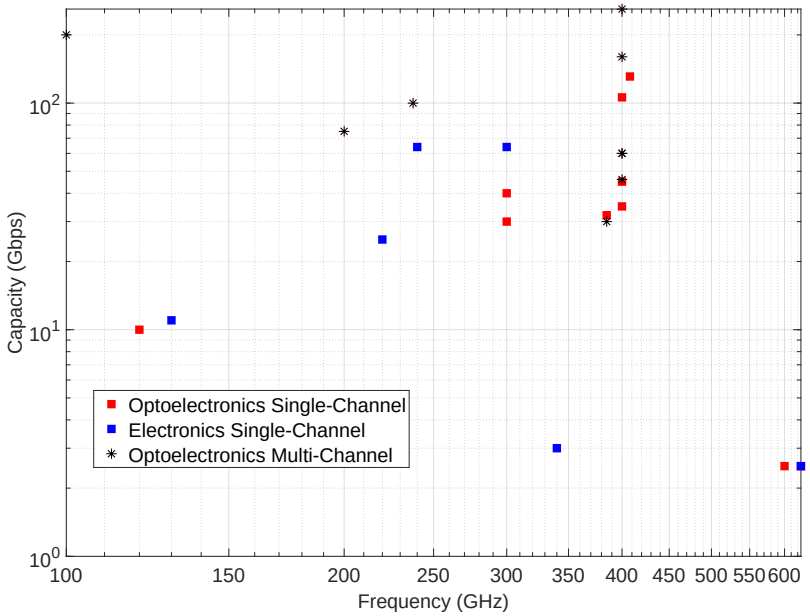

Figure 7: State-of-the-art of sub-THz wireless communications research. Blue and red squares are single-channel electronics and single-channel optoelectronics solutions. Black asterisks are multi-channel optoeletronics solutions. References used: [14][15][16][17][18][19][20][21][22][23][24][25][26][27][28][29][30][31][32][33][34][35][36][37]

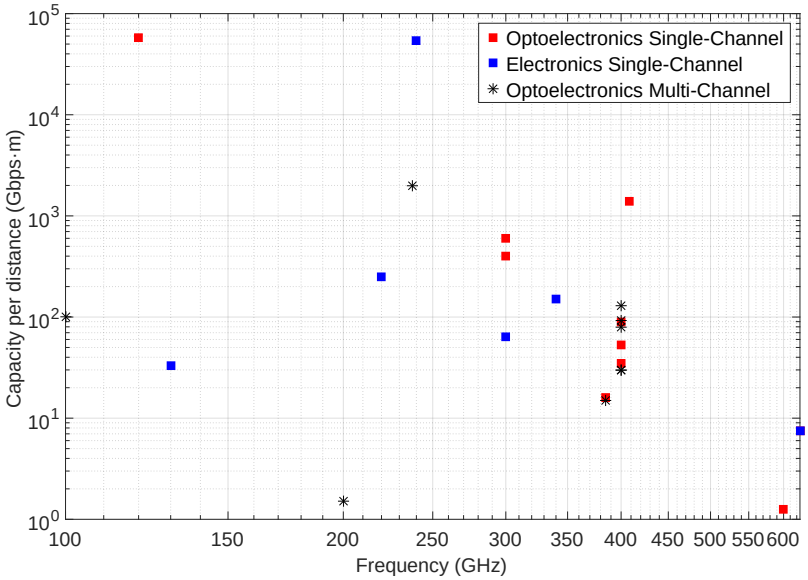

Figure 8: Figure 7 with figure of merit *capacity x distance*. Blue and red squares are single-channel electronics and single-channel optoelectronics solutions. Black asterisks are multi-channel optoeletronics solutions.

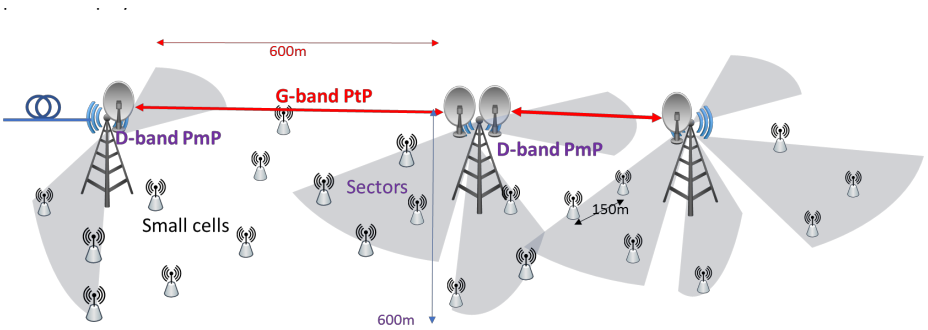

Figure 9: ULTRAWAVE's link proposal.

This amplifier is a brand new device that can provide power at Watt level in D/G-bands, in fact, provides 40 dB and 30 dB respectively, being a key component in the quest of improving *capacity x distance product* [38].

Within this project, the role played by the Universitat Politècnica de València is the design and development of a generation system of G-band signals that will feed the PtP links using photonic techniques to provide stable signals carrying the requested data rates. The present document summarizes some of the work carried out to reach this objective.

A generic photonic generation system would be similar to Figure 10, where an optical comb is generated, several spectral lines are demultiplexed and modulated (remaining one as an local oscillator), combined and photodetected.

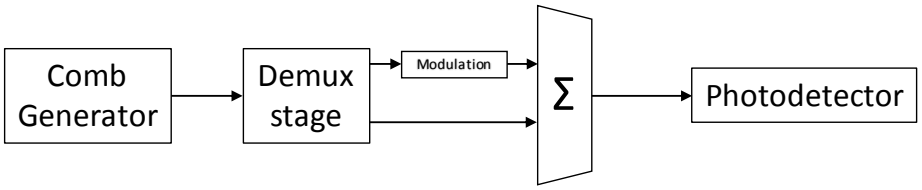

Figure 10: Generic photonic generation system.

This document presents the characterization of the photonic system. The potential performance is assessed and critical design limitations are identified. The remainder is organized as follows: first various possible architectures are evaluated and one is chosen, second an analog characterization is performed with theoretical and experimental results, third a digital characterization using VPIphotonics software is used to delimit which features (such as channel spacing, number of channels, etc.) affect more the whole system and finally conclusions are stated.

2 Proposed architecture

Keeping in mind the different techniques presented at the Introduction, the coherent optical source chosen for this work is external modulation of a CW laser with two cascaded

phase modulators (PM) because its ease of implementation, phase quality and devices available at the lab.

Once comb is generated, two optical tones are demultiplexed and this section presents different the four options that have been considered for demultiplexing stage at the photonic generation system. All of them are based on external modulation of a CW laser with two PM for generating an optical comb boosted by an EDFA. The difference between them lies in using distinct demultiplex components, namely wavelength selective switch (WSS), arrayed waveguide grating (AWG), fiber Bragg gratings (FBG) and a combination of FBG and an optical demultiplexer (Figures 11 to 13).

In order to decide, a trade-off between cost and losses must be achieved considering the following:

- WSS: the most straightforward way. All optical channels suffer same attenuation but it is the most expensive and bulkier configuration (Figure 11).
- AWG: it is more economical than WSS but it lacks reconfigurability and the granularity of the channels is considerably larger than WSS. In addition, it must be taken into account the periodicity between ports (Figure 11).
- FBGs: the most affordable. Useful for testing and measurement. Lacks in scalability due to different attenuation between channels (Figure 12).
- FBG+Demux: middle term solution. Local oscillator (LO) and optical channels suffer different attenuation but very cheap compared to WSS. Once the demux is placed it is not possible to transmit more channels so it lacks in upper scalability (Figure 13).

Considering that the main objective is to build a proof-of-concept (having an irregular comb and transmitting only one optical channel), the best option is to use two FBGs (for LO and transmitting channel) which brings simplicity to the setup at a very low cost. Once demux stage is fixed, LO and transmitting channel are recombined and amplified again before launching them into the UTC-PD.

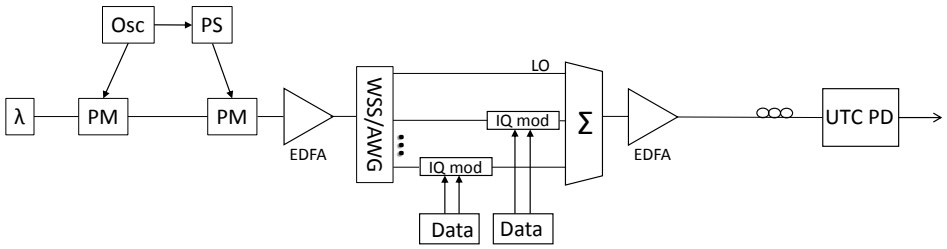

Figure 11: Proposed architecture using a WSS/AWG for demultiplexing.

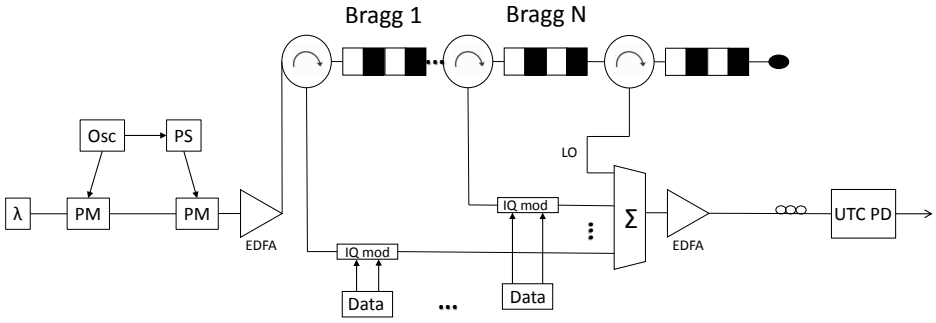

Figure 12: Proposed architecture using Bragg gratings for demultiplexing.

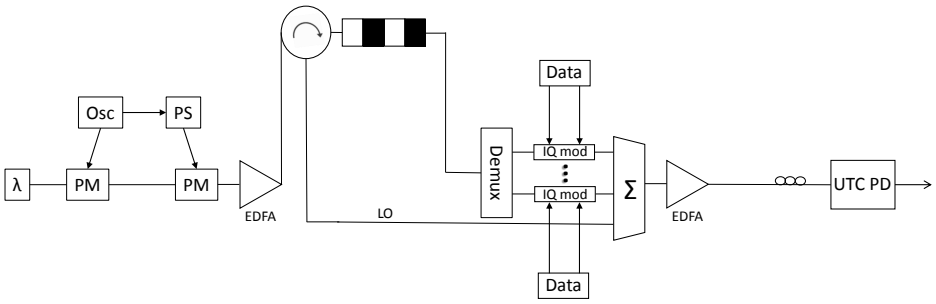

Figure 13: Proposed architecture using one Bragg grating and a demultiplexer for demultiplexing.

3 Analog characterization

In this section, an analog characterization of the photonic transmitter is performed so that the system is characterized both theoretically and experimentally.

3.1 Link budget

The link budget for the architecture described in Section 2 is performed. First, the laser optical output field can be written as,

$$E_{in} = \sqrt{2P} \cdot e^{j2\pi f_c t} \tag{1}$$

where P is the optical power and f_c is the frequency of emission [39]. Then, light goes through each phase modulator, which are fed using a RF signal with a frequency of f_{RF}. Thus, to generate a wider optical comb, more RF power is needed, however since the output electrical power of an amplifier and the amount of RF power that a phase modulator can handle are limited, the use of two cascaded PM is required [40], inasmuch as the system demands a good level of the +/-6th harmonics.

With that being said and knowing that drive RF signals are $f_1 = R_1 V_\pi sin(2\pi f_{RF} t)$ and $f_2 = R_2 V_\pi sin(2\pi f_{RF} t + \Delta\theta)$, ($\Delta\theta$ and V_π are the phase deviation between drive signals and the half wave voltage respectively) the field at the output of the second modulator can be expressed as follows

$$E_{out} = \frac{Ein}{L_{PM}} \cdot e^{j\pi R_c sin(2\pi f_{RF} t + \varphi)} \approx \frac{\sqrt{2P}}{L_{PM}} \sum_{n=-m}^{m} J_n(\pi R_c) \cdot e^{j2\pi(f_c + n f_{RF})t + n\varphi} \tag{2}$$

where πR_c, J_n, L_{PM} and φ are the combined modulation index, the Bessel function of the first kind and order n, PM insertion losses and phase noise of the RF signal respectively. Expression for R_c is derived to be

$$R_c = \sqrt{R_1^2 + 2R_1 R_2 cos\Delta\theta + R_2^2} \tag{3}$$

which determines the level of the carriers that compose the optical comb [40].

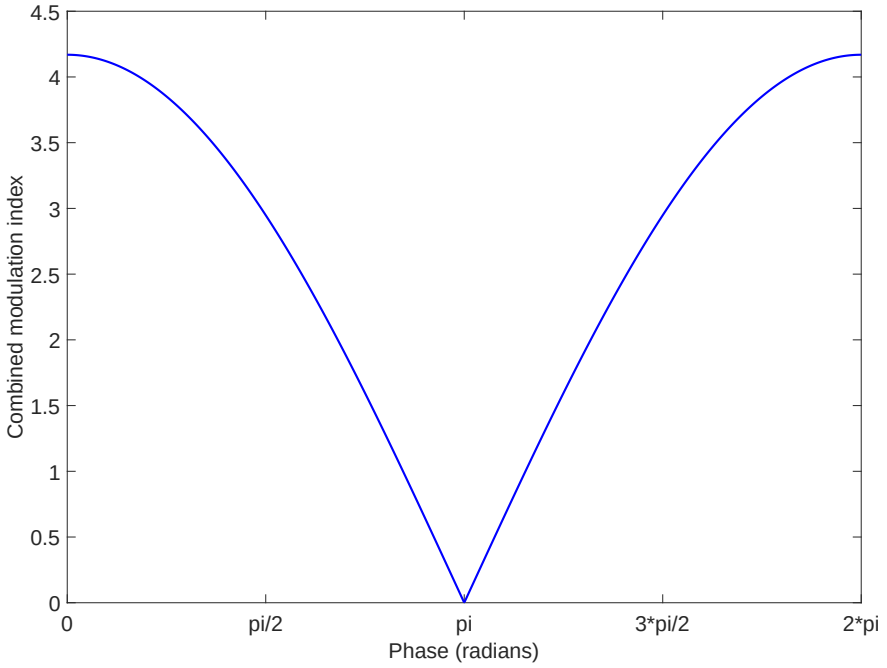

Figure 14: Combined modulation index related to phase deviation of the drive signals.

From equation (3) and Figure 14 it can be seen that compensating the deviation phase of the RF signals results in higher levels of carriers away from the central frequency, which turns out into better signal at G-band. This is the reason why in Figures 11, 12 and 13 an electrical phase shifter (PS) is included before the second PM. Note that an electrical and not an optical one is used because, as can be seen in Figure 15, the electrical option has lower losses, i.e. better power for the desired harmonic.

A theoretical study to define the required power of the microwave local oscillator driving the PMs has been performed. Figure 16 shows the dependence of the 6th harmonic power

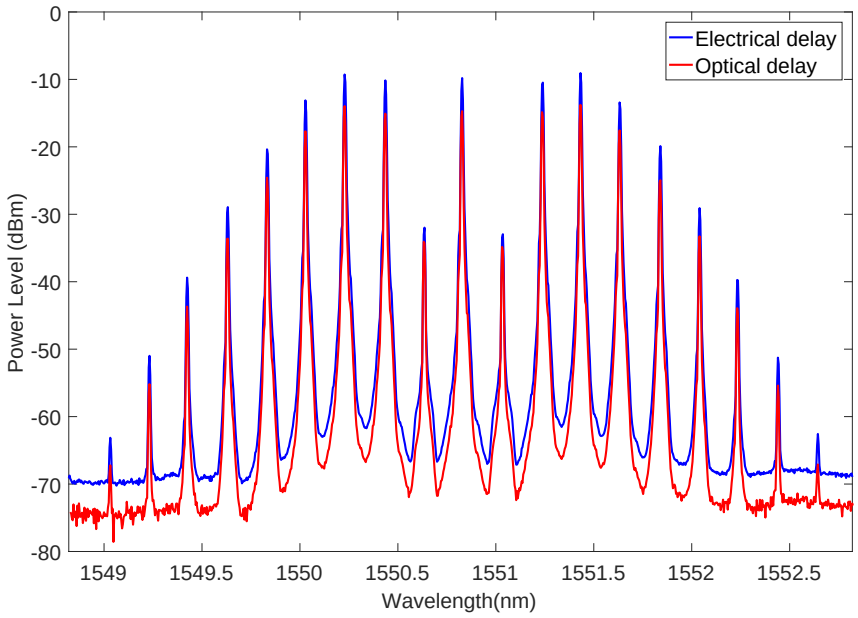

Figure 15: Optical comb generated using electrical (blue) and optical (red) delay.

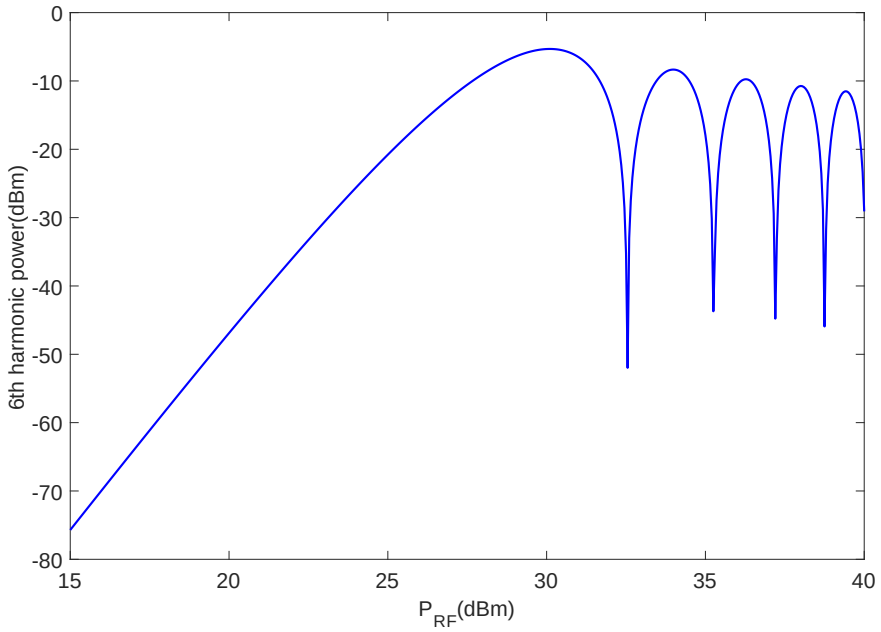

Figure 16: 6th harmonic power vs RF power used at external modulation.

as a function of the microwave LO. Taking into account the saturation of the electrical amplifier, the target power for the microwave oscillator has been set at 25 dBm. Figures 17 and 18 show the power of the optical comb, theoretical and experimental results,

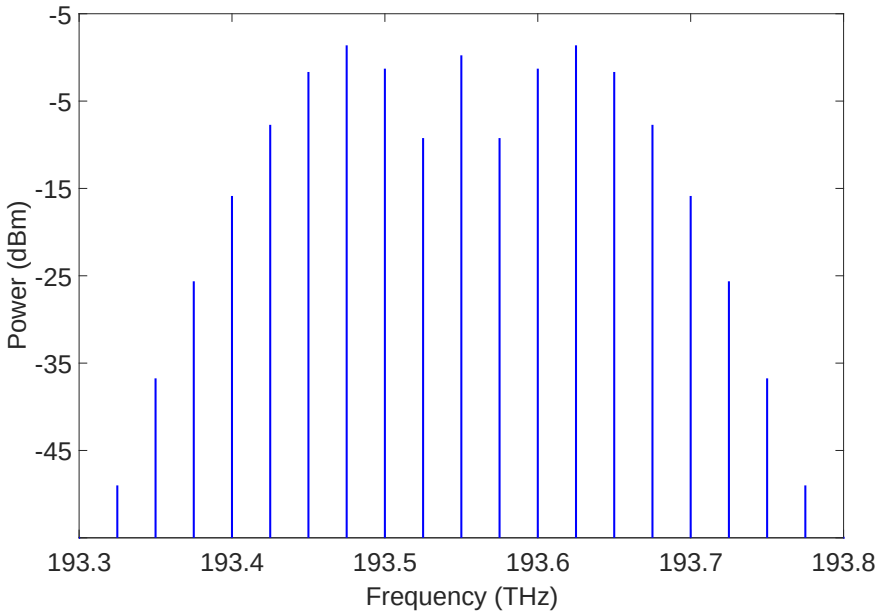

Figure 17: Optical comb generated using equation (2).

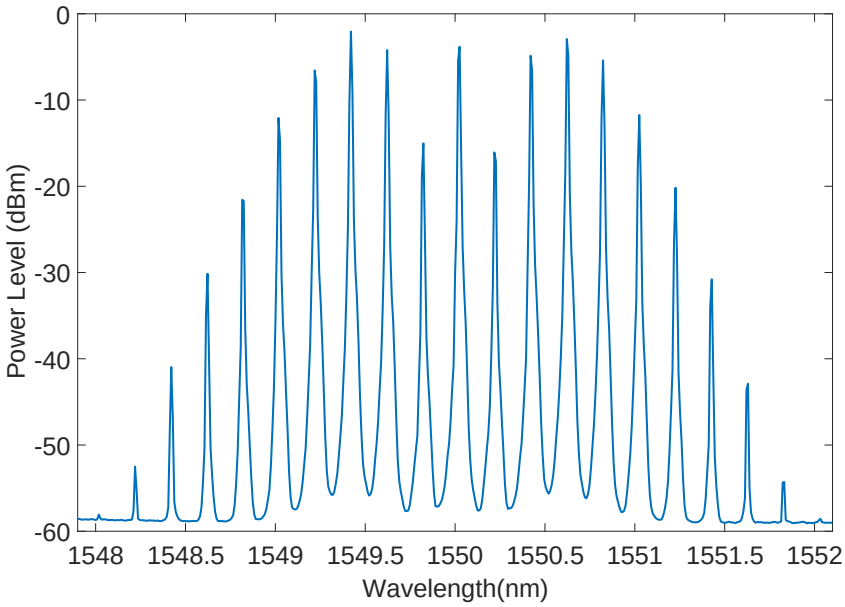

Figure 18: Optical comb generated using the experimental setup.

respectively, using an optical source with an output power of 13 dBm. Table 1 gives an overview about how similar are the experimental measures against theoretical ones, being the largest difference 0.7dB corresponding to the 9th harmonic, what can be considered as a good agreement.

Harmonic	Experimental SNR (dB)	Theoretical SNR (dB)
1st	46.5	46.8
2nd	55.3	54.78
3rd	57.5	57.45
4th	54.1	54.4
5th	48.5	48.35
6th	39.6	40.2
7th	29.9	30.44
8th	18.8	19.32
9th	6.3	7

Table 1: Comparative of SNR at the optical comb between theoretical and experimental results. The theoretical noise floor is assumed to be the same as the experimental (-59 dBm).

Next, a link budget is performed to guarantee proper operation of all the components used. Figure 19 shows the result, where blue values correspond to theory and red ones to measured data.

Finally, the whole photonic transmiter has been tested. Since a spectrum analyzer with a bandwidth of 300 GHz is not available at the lab, a subharmonic mixer has been used for downconverting the signal to IF band, which incurs in significant losses, 30-50 dB. The particular losses are not available yet. To get the IF signal, a 18.688 GHz signal is used as local oscillator in the mixer to achieve the 16th harmonic at 1 GHz. On this basis, the power after the UTC (and before downconversion) is calculated using the following equation

$$P_{RF} = 2\Re^2 Z_L P_{upper} P_{lower} \tag{4}$$

where $\Re$ is the responsivity of the photodiode, Z_L is the load impedance and $P_{upper/lower}$ is the power of the two tones that arrive to UTC [41] (the parameters used are described in Table 3 in Appendix A). Figure 20 shows the downconverted generated tone (not carrying data) with a peak power of nearly -65 dBm, which is around 40 dB lower than the photodetected one, which agrees with the specifications of the subharmonic mixer provider.

3.2 Noise characterization

Noise degradation appears due to multiple factors in a fiber optics systems and can be measured at different points of the link. In this work, the expressions focus on the carrier to noise ratio (CNR) and phase noise at the output of the UTC-PD, which are the parameters that characterize the quality of a signal carrying data.

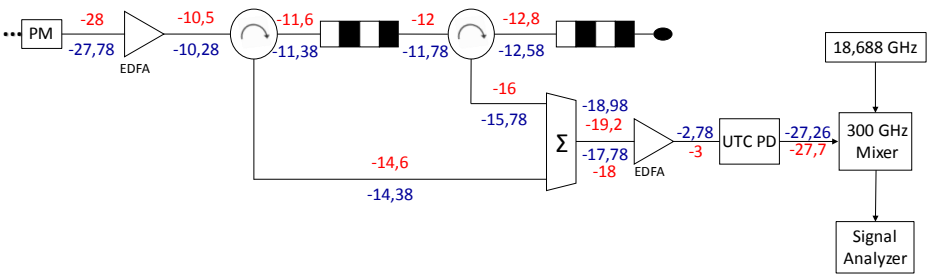

Figure 19: Link budget of the system both experimental (red) and theoretical (blue). All levels are in dBm.

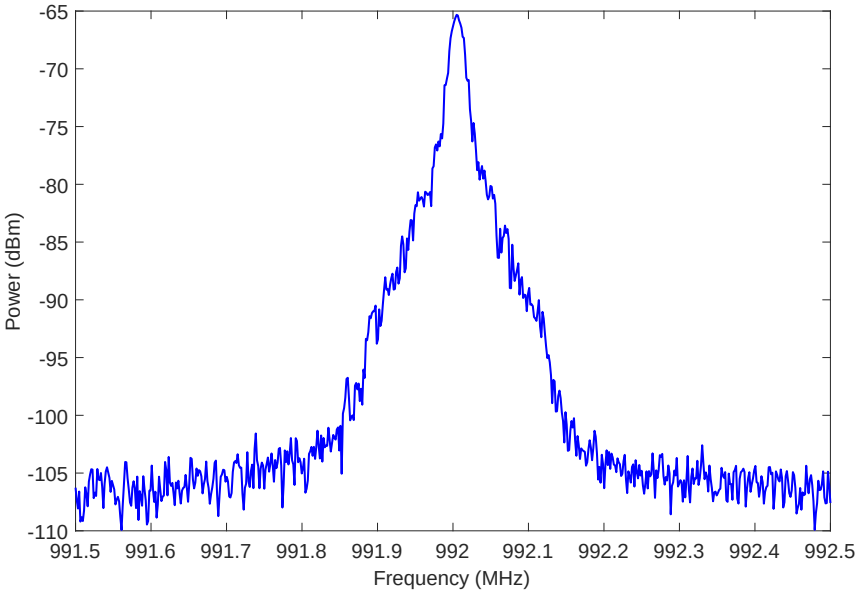

Figure 20: Photonically generated 300 GHz carrier downconverted to 1 GHz.

3.2.1 Thermal noise

Thermal noise is related to the fact that electrons move randomly along the load resistance of the photodetector and can be written as follows

$$\sigma_{th}^2 = \frac{4kT_0\Delta f F}{Z_L} \tag{5}$$

where k is the Boltzman constant, T_0 is the ambient temperature, Δf is the electrical bandwidth and F is the total noise factor of the amplifying stages.

3.2.2 Shot noise

Shot noise depends on the average optical power measured at the input of the photodetector and it is originated from the quantum nature of the photodetection process.

The equation is derived as

$$\sigma^2_{shot} = 2q(I_p + I_d)\Delta f \tag{6}$$

where q is the electron charge, I_p is the average photocurrent and I_d is the dark current.

3.2.3 RIN noise

Relative intensity noise (RIN) comes from intensity fluctuations at the optical signal generated by the laser. Considering that RIN parameter is constant at the considered bandwidth, the expression is written as follows

$$\sigma^2_{RIN} = RIN_{laser}(I_p)^2\Delta f \tag{7}$$

where RIN_{laser} is the RIN parameter of the laser.

3.2.4 EDFA noise

Erbium doped fiber amplifier (EDFA) are widely used and known in optical systems for compensating losses but this results in noise degradation too, owing to the fact that amplified spontaneous emission (ASE) occurs at the amplification stage. This has a direct effect incrementing the shot noise and provoking beatings between spontaneous signal with itself, with the signal and with the shot noise.

First of all, EDFA has a noise spectral density because of spontaneous emission

$$S_{sp} = (G-1)n_{sp}hf_c \tag{8}$$

where G is the gain, n_{sp} is the population inversion factor and h is the Planck's constant. Before reaching the photodetector the noise spectrum is modified in a way that can be written as

$$S_{sp_{mod}} = \frac{S_{sp}}{L} \tag{9}$$

where L are the losses from EDFA to the photodetector.

Secondly, the beatings (spontaneous with itself, signal and shot) are expressed as

$$\sigma^2_{sp-sp} = 4\mathfrak{R}^2 S^2_{sp_{mod}}\Delta\nu\Delta f \tag{10}$$

$$\sigma^2_{sig-sp} = 4\mathfrak{R}^2 S_{sp_{mod}}P_o\Delta f \tag{11}$$

$$\sigma^2_{s-sp} = 4q\mathfrak{R}S_{sp_{mod}}\Delta\nu\Delta f \tag{12}$$

where $\Delta\nu$ is the bandwidth of the EDFA.

Thirdly, the increment of shot noise can be scripted as follows

$$\sigma^2_{shot} = 2q(\mathfrak{R}(P_o + S_{sp_{mod}}\Delta\nu) + I_d)\Delta f \tag{13}$$

Finally, after the photodetection, all the noise can be gathered in one term σ^2 (the sum of all of the sources mentioned before) which contributes to the CNR equation as follows

$$CNR = \frac{P_{carrier}}{\sigma^2} \tag{14}$$

where $P_{carrier}$ is the RF power of the modulated signal[42][41]. Estimations have been calculated with the parameters in Table 3 of Appendix A and are depicted in Figure 21. It is important to note that the physical system uses 25 dBm as RF power that is translated into 4.169 combined modulation index, corresponding to 30.36 dB of CNR and data modulation is considered, conversely to link budget experimental estimations.

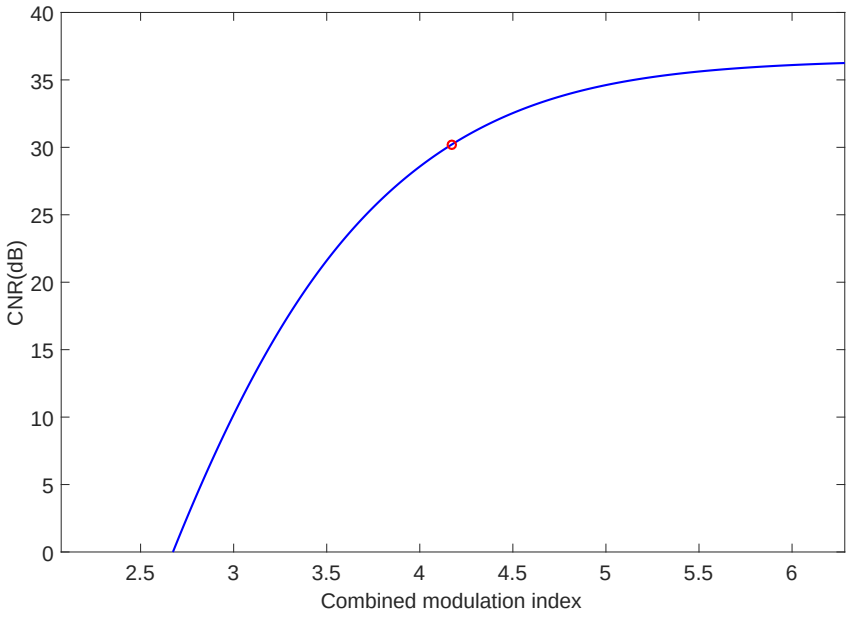

Figure 21: CNR vs combined modulation index. Red circle highligths the working point.

3.2.5 Phase noise

Phase noise is a phenomenon unavoidably present in oscillators in general, affecting generated tones too, and is produced owing to the fact that the power of an electromagnetic wave does not remain immutable at a single frequency. On the contrary, it is spread across a distribution of frequencies causing several unwanted issues such as constellation rotation, interference masking and jitter among others. Equation 15 and Figure 22 are mathematical and graphical examples of the effect of phase noise [43].

$$E(t) = E_0 \cos\left(2\pi f_0 t + \phi(t)\right) \tag{15}$$

Focusing on the characterization of phase noise at G-band tones generated via photonic transmitters, Shao et. al. in [44] and [45] studied thoroughly which are the main contributions to it, demonstrating the following equation

$$\phi_{Photonic-RF} = n\phi_{LO}(t) \tag{16}$$

where $\phi_{Photonic-RF}$ represents the phase noise of the G-band signal, $\phi_{LO}(t)$ represents the phase noise of the oscillator feeding PMs and n is a real number that depends on the

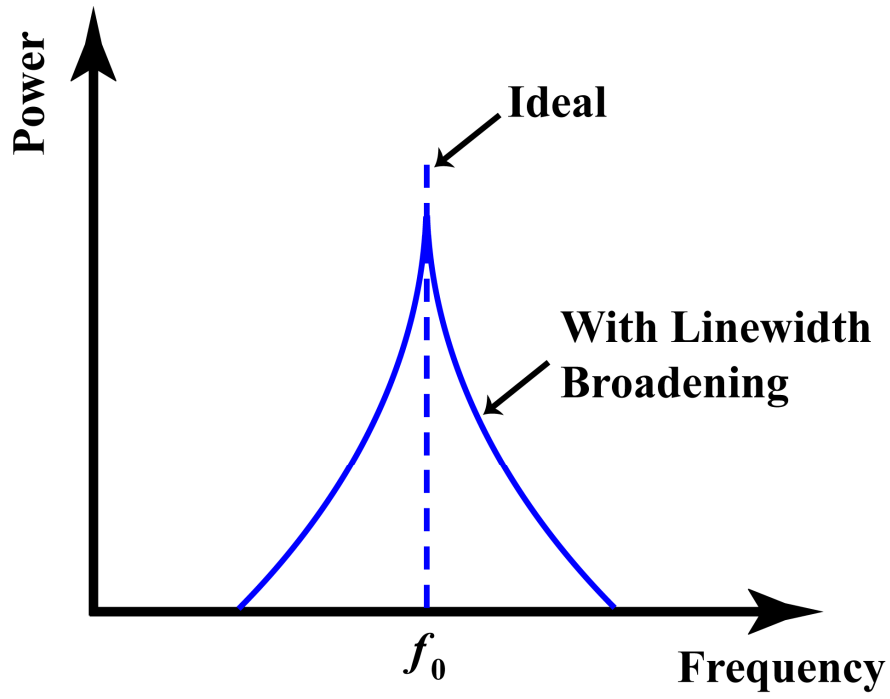

Figure 22: Graphical example of phase noise.

comb harmonics that are mixed at the photodetector (12 in the current case since +/- 6th harmonics are used). Note that laser's linewidth is not involved with the resultant broadening and also the downconversion process adds phase noise. Figures 23 and 24 show the measurements.

In light of the previous graphs, a degradation of around 30 dB in Figure 23 can be seen from 25 GHz oscillator (blue) to G-band tone generated (red), where 20 dB are predicted using equation 16 (dashed blue). The remaining difference cannot only be accounted to phase noise introduced at downconversion stage since the phase noise of the 25 GHz oscillator is >3 dB than the 18.688 GHz one so another factor is impairing the signal. In [45] is mentioned that this aspect is related to the time delay between the two optical paths that decorrelates the phase of the harmonics demultiplexed and can be corrected adding fiber to one path as done in [44]. 2 meters of fiber have been added in order to correct it, obtaining a result (black) close to theoretical degradation.

3.3 Linearity

As mentioned in [46] and [47], a significant parameter to measure the linearity of a RoF system is the spurious free dynamic range (SFDR) and is mainly limited by the nonlinear transfer function of a Mach-Zehnder modulator (MZM). That is to say, measuring the SFDR of the Mach-Zehnder alone gives a good approximation of the whole link. In the current case, the setup used can be seen in Figure 25. The UTC is not the photodetec-

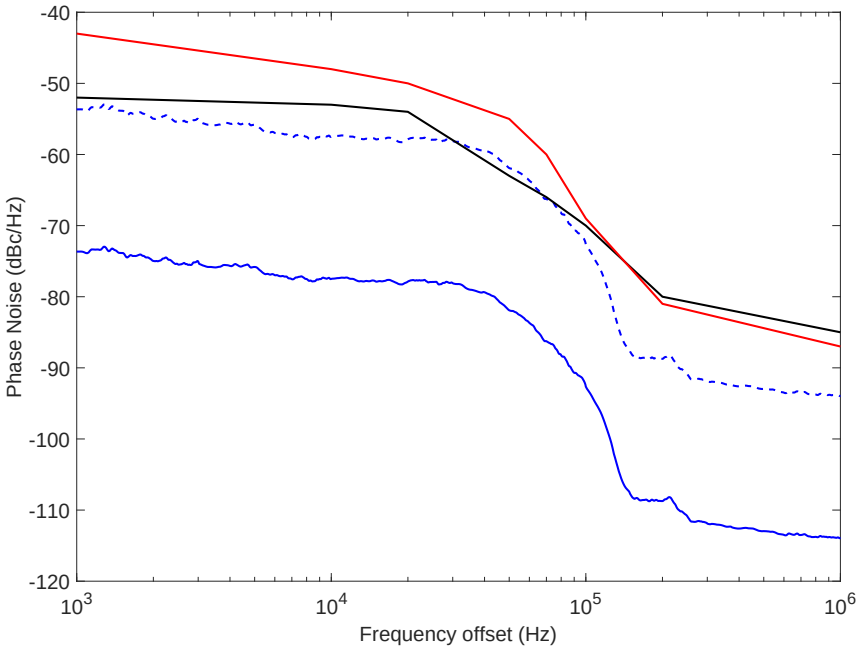

Figure 23: 25 GHz oscillator (blue), G-band tone (red) and 2 m of fiber compensation (black) measured phase noise. 25 GHz oscillator phase noise degradation predicted with equation 16 (dash red).

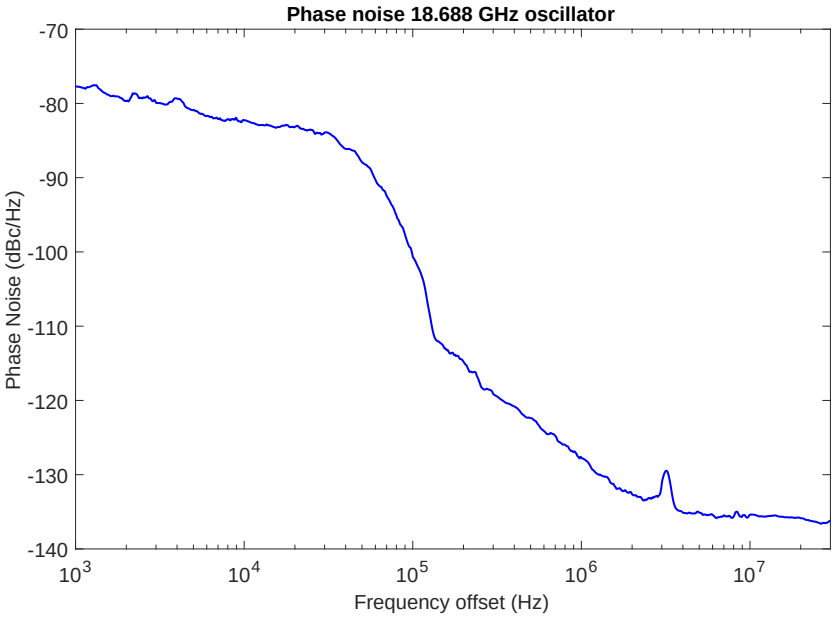

Figure 24: 18.688 GHz oscillator measured phase noise.

tor because its bandwidth would compel to downconvert the RF signals, corrupting the measure of the SFDR so instead, an standard photodiode with 0.7 A/W responsivity and 9 GHz high-frequency cut off is used. It is important to note that the modulator used is a dual-parallel Mach-Zehnder (DP-MZM), whose parameters are described in Table 3 of Appendix A.

The process to measure SFDR is the following:

1. Both arms of the DP-MZM are polarized at quadrature point [47].
2. Two tones at frequencies 4 and 5 GHz feed the modulator, generating a third order intermodulation product at 6 GHz, which is monitored with FSQ 40 signal analyzer.
3. RF power is varied in order to have several points for knowing how fundamental and third order intermodulation signals vary. This can be seen in Figure 26 and the information extracted is summarized in Table 2.

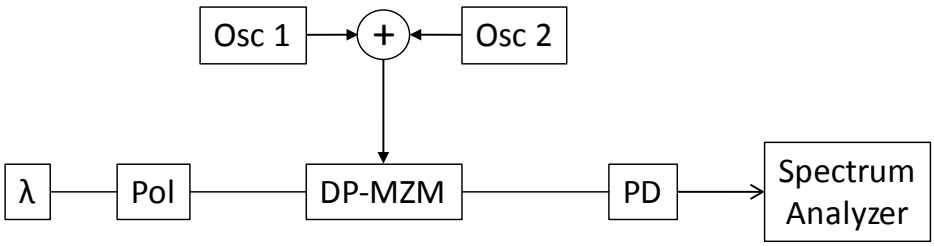

Figure 25: Setup used to measure linearity of the system.

IIP3	OIP3	SFDR	G_{link}
14 dBm	-5.4 dBm	88 dB · $Hz^{2/3}$	-20.4 dB

Table 2: Information extracted from Figure 26. OIP3 stands for third order output intermodulation point and IIP3 for third order input intermodulation point.

Once SFDR is measured, theoretical value is calculated using the equations 17 and 18 from [48] and [49]

$$SFDR = \frac{2}{3}\left(IIP3 - (N_{th} + NF)\right) \tag{17}$$

$$NF = N_{th} + N_{floor} - G_{link} \tag{18}$$

where N_{th} is thermal noise (-174 dBm), N_{floor} is the link noise floor and NF is the noise figure of the link. The value obtained is around 90 dB · $Hz^{2/3}$.

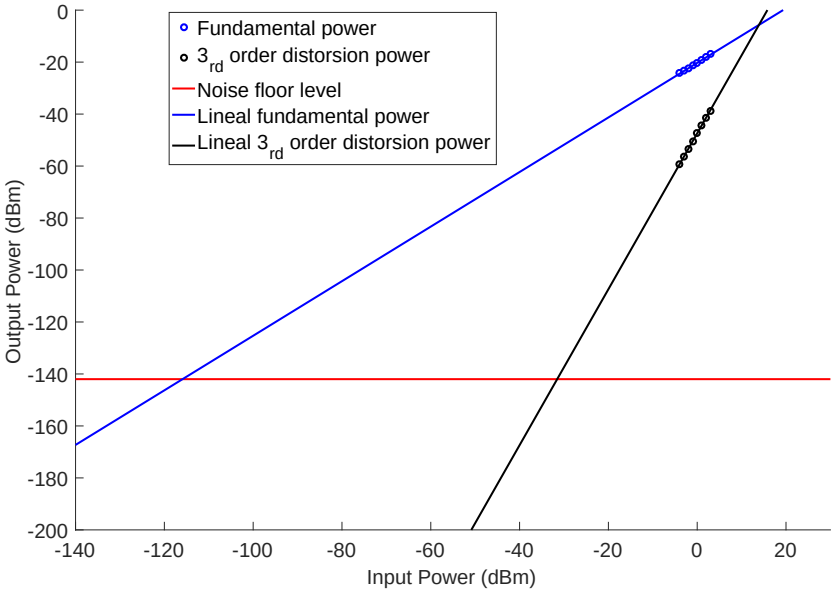

Figure 26: Fundamental power (blue) vs third order distorsion (black) to calculate SFDR.

4 Digital characterization

With the objective of assessing the performance to be achieved by the photonic transmitter, simulations are performed using VPIphotonics software, which is a widely known software to design and simulate optical systems.

The VPI schematic is similar to Figure 12 but only with two FBGs and one Mach-Zehnder (standard modulation) modulating four electrical channels onto the optical signal (the result can be seen on Figure 27). It is important to note that, even though the optical comb is generated with two cascaded PM at the lab, here a standard MZM is used since real PMs are not included in *VPIphotonics design suite*.

In optical communications, one of the most important figures of merit that characterizes an advanced data transmission is EVM, which stands for error vector magnitude. It basically measures the distance of the received symbols from its ideal position [50][51].

$$EVM_{RMS} = \frac{\frac{1}{N}\sum_{n=1}^{N}|S_n - S_{0,n}|^2}{\frac{1}{N}\sum_{n=1}^{N}|S_{0,n}|^2} \tag{19}$$

where N is the number of unique symbols in the constellation, $S_{0,n}$ is the ideal normalized constellation point of the nth symbol and S_n is the normalized nth symbol in the stream of measured symbols.

Ideal environment yields a 0% EVM and, when real parameters are introduced (noise, non-linearities, etc.), it degrades significantly. The goal here is to find out which are the main parameters that corrupt data transmission and delimit them for future practical

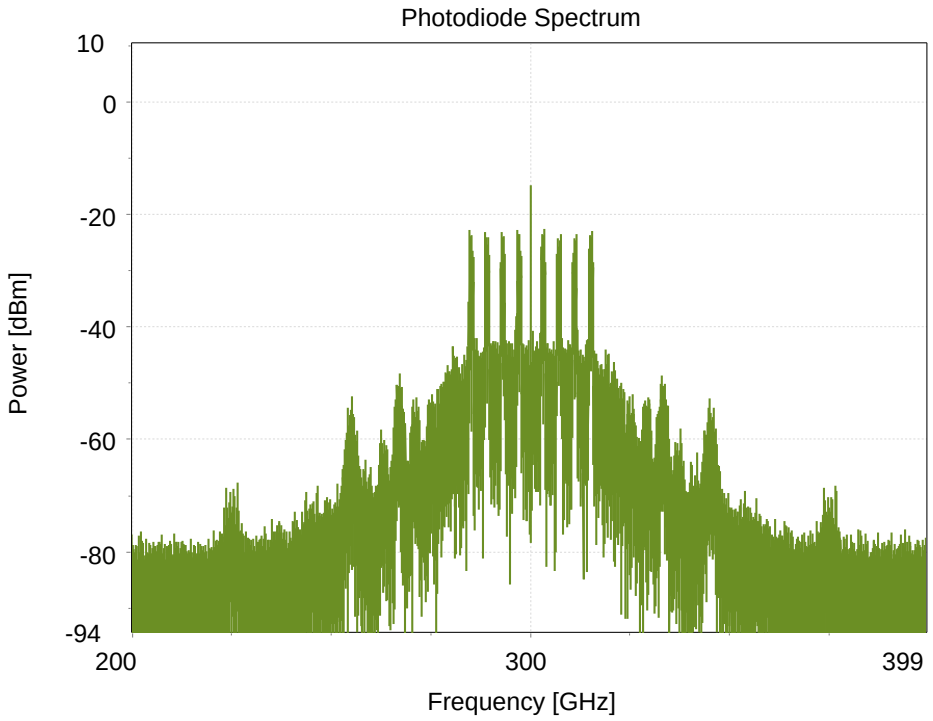

Figure 27: Spectrum of the electrical signal after photodetection simulation with Pin=13dBm.

work. All the following Figures are extracted using (parameters under study may vary) the following considerations: channel 2 evaluation, Table 3 parameters of Appendix A, 2 Gbps data rate, QPSK modulation, four electrical channels (3, 7, 11 and 15 GHz) and channel spacing equal to 4 GHz.

4.1 Parameters variation

In view of Figure 28 it is clearly observed that input laser power is a critical parameter regarding EVM performance. It is due to the importance of the harmonic level for the generation of the G-band signal. Furthermore, a saturation with high powers is seen because of, as explained in [50], EVM is related to SNR and around 22 dBm more input power causes to augment both signal and noise. With that being said and knowing the limitations of maximum input power of system devices, 13-16 dBm as input power seems to be reasonable tradeoff.

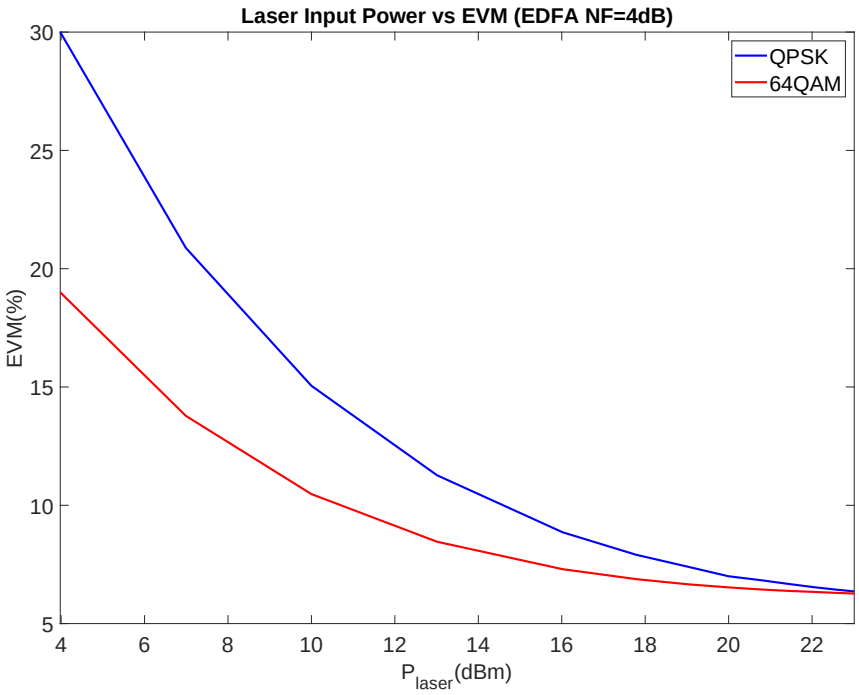

Figure 28: EVM versus laser input power for channel 2.

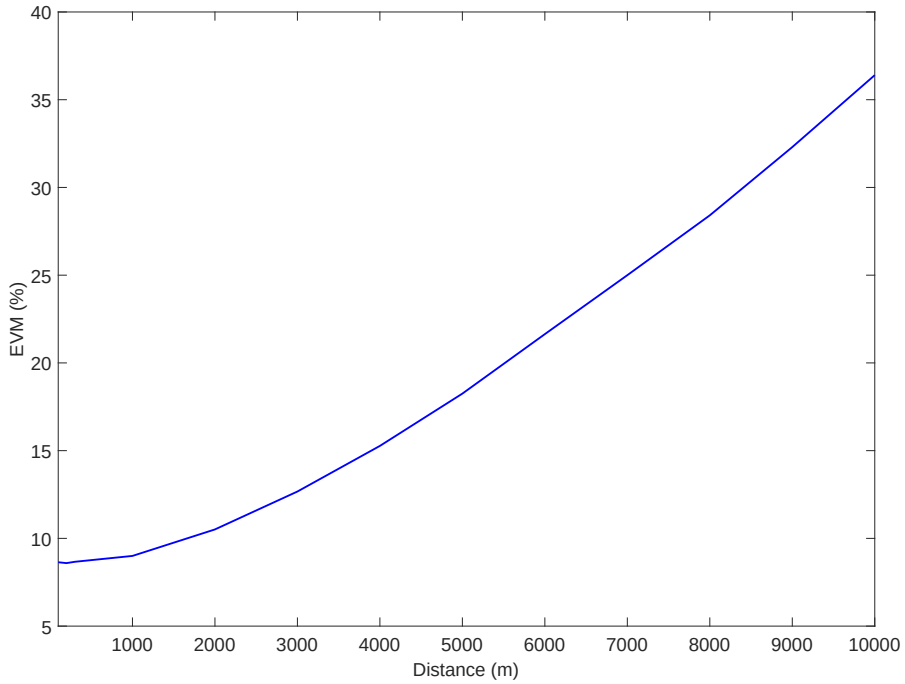

Figure 29: EVM versus SMF-28 Corning standard single mode fiber length.

As observed in Figure 29, fiber length before photodetection is a critical parameter

that must be taken into account since it can destroy the capabilities of the link.

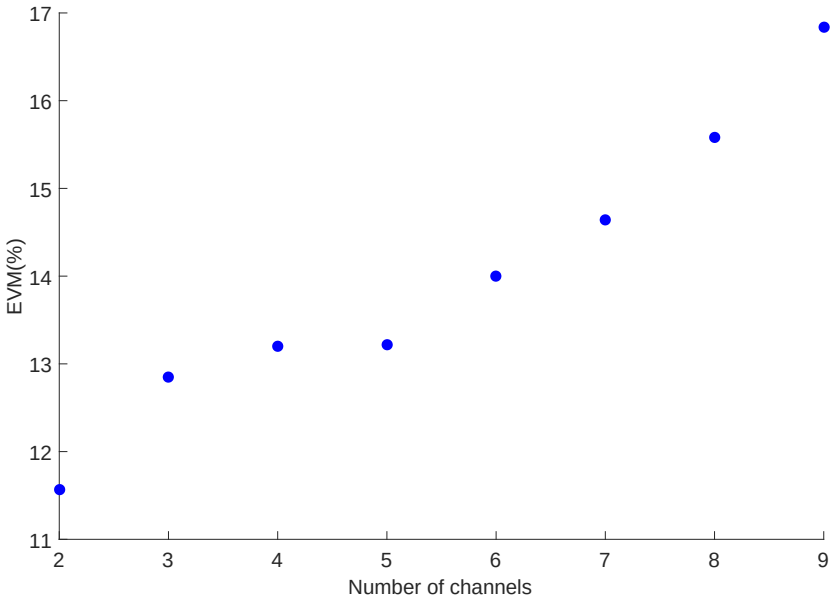

Figure 30: EVM versus number of channels transmitted for channel 2.

In Figure 30 a relationship between EVM and number of channels transmitted is established. Here it is clear that crosstalk from other channels affects the performance so the more channels you transmit, the more crosstalk is induced. Current conditions lead to transmit four or five channels but this is extremely related to data rate and spacing (next parameters to be discussed) so depending on requirements different options would be correct.

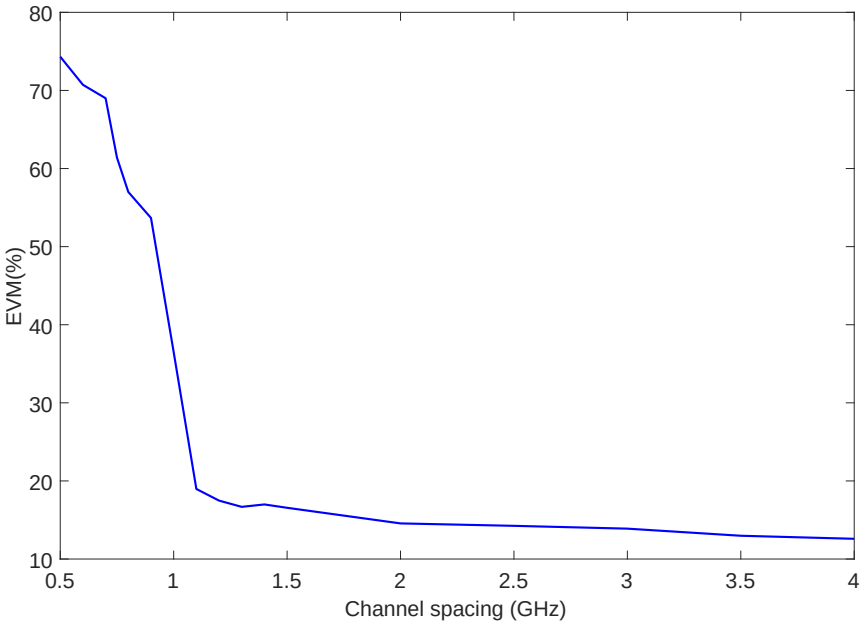

Figure 31: EVM versus four channels spacing for channel 2.

Regarding channel spacing, Figure 31 focuses on it. With a data rate of 2 Gbps it is easy to say that at least 1.5 GHz of guard band is needed, recommending 2 GHz. As expected and discussed in relation to Figure 30, the number of channels and data rate play a role in determining the correct channels spacing.

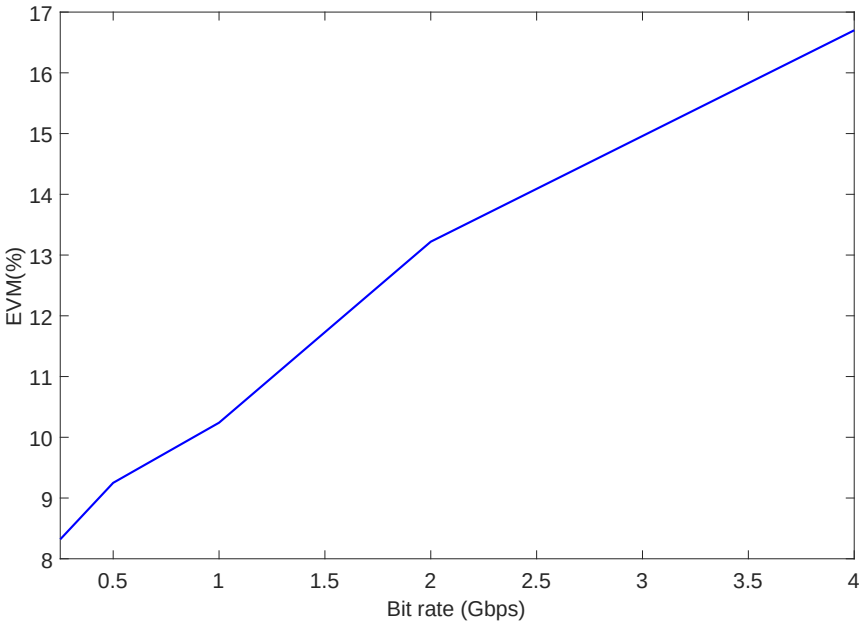

Figure 32: EVM versus bit rate for channel 2.

Finally, a relation between data rate and EVM is depicted in Figure 32. As expected, higher data rates broaden the channel spectrum, requiring larger channel spacing to keep crosstalk and EVM constant.

4.2 Discussion

In light of the previous graphs, on the one hand, one of the parameters that affect more EVM is the laser input power, which translates into better level of harmonics +/-6. In fact, not only the laser limits this but the modulation index applied to generate the comb, that is to say, having higher power signal at the harmonics improves the quality of the data transmission since better CNR is achieved. The following lines shed light on this issue.

Firstly, rising the optical power by means of more laser input power can be a mid-term improvement, but all the devices have a maximum that can handle and better lasers are more expensive, so when designing the system this has to be taken into account. Secondly, getting more modulation index with more RF power it is definitely not easy since standard amplifiers typically sature at the required output power (25 dBm at 25GHz). PM modulators cannot be fed with much more and cascade another PM raises the price of the system. Some more complex setups have been proposed [52] and [53] to achieve flatter and broader optical combs. Knowing that the current work is a proof-of-concept, this is momentarily dismissed but is going to be a main topic in future work. Thirdly, state-of-the-art UTC-PDs cannot give more than -10 dBm so more efficient sub-THz photodiodes need to be developed.

On the other hand, a trade off between channels spacing, number of channels transmitted and data rate needs to be settled. Transmitting more channels means more crosstalk so more spacing will be needed (occupying more spectrum consequently) with appropriate data rate.

Finally, an important relationship between fiber length and EVM is denoted. Due to operation in the G-band direct radio-over-fiber transmission is not straightforward and this effect is attributed to phase-to-intensity noise conversion. Thus, although no carrier suppression is induced in the system thanks to beatings of sidebands with carrier signal are out of G-band, dispersion shifted fibers should be used to allow remote delivery of G-band signals across long distances. The relative delay is calculated as

$$\tau_0 = DL\Delta\lambda \tag{20}$$

where D is chromatic dispersion parameter, L is the total optical fiber length and $\Delta\lambda$ is the separation between tones [54]. Knowing that SMF-28 dispersion is $17\frac{ps}{nmkm}$ in third window and optical tones are separated 2.4 nm away, equation 20 can be written as

$$\tau_0 = 40.8L\left[\frac{ps}{km}\right] \tag{21}$$

The deterioration of the constellation can be observed in Figure 33 as an intensity noise induced by this time delay. Particularly, this effect seems to be more deleterious than the

one observed in other optical heterodyne systems and the reason behind this is that the G-band signal is generated through the beating of two optical comb lines separated 2.4 nm (300 GHz), converting it into a singularity of the system proposed. In [54], similar to what is described in [45], an alternative to reduce the impact of the time delay is to pre-compensate with a tunable optical delay and will be implemented when practical data transmission is carried out.

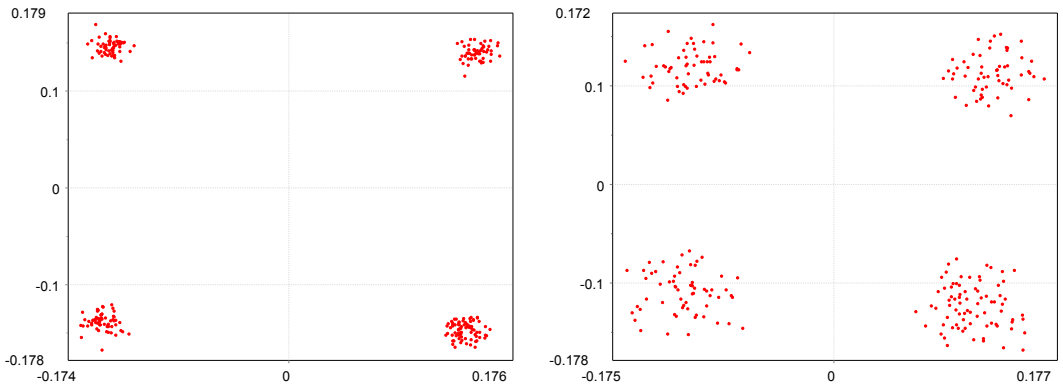

Figure 33: Left: QPSK constellation after 1km SMF-28 Corning ($EVM \approx 9\%$). Right: QPSK constellation after 5km SMF-28 Corning ($EVM \approx 18\%$).

5 Conclusions

In this Master Thesis an optical-assisted generation system of G-band signals has been characterized both theoretically and experimentally. Once the setup is decided, analog and digital results are presented where the capabilities and limits of the proposal are assessed:

1. A laser between 13-16 dBm output power is ideal to get maximum benefit without impairing other devices or waste energy. Furthermore, and RF power of 25 dBm is used to generate the optical comb, being this value the maximum that the RF amplifier at the lab can get. One important topic in the future will be how to generate higher optical tones away from the center wavelength without using more RF or optical power, inasmuch as impacts directly to the performance of the whole system.

2. Phase noise degradation is generated by beating of optical tones that go through different optical paths and harmonics beating. The first is corrected adding 2 meters of fiber.

3. A CNR of around 30 dB is expected using the DP-MZM described in Table 3 in Appendix A. Practical data transmission will be carried out in future work.

4. Because of high frequency generation, effects of fiber length must be taken into account, since degrade the transmission severely. 1km yields around 9% of EVM and 5km yields 18%. Similar to fiber compensation, a tunable optical delay line will be used to soften this impairment.

5. In software simulation, four channels at frequencies 3, 7, 11 and 15 GHz are transmitted with 2Gbps data rate and QPSK modulation. Up to five channels can be transmitted without significant degradation if at least 1.5 GHz spacing between them is guaranteed, that is to say, depending on the requirements of data transmission, a trade-off between number of channels, data rate and spacing needs to be set in order to ensure proper operation.

6 Acknowledgements

The current project would not be possible without the support of the European Union's Horizon 2020 research and innovation program. I would like to thank the Universitat Politècnica de València and, specifically, the Nanophotonics Technology Center for its trust and for giving me an opportunity to develop my professional career working in a reputable environment full of great experts.

Individually, I cannot forget to acknowledge my master thesis director Borja Vidal for his wisdom and guidance throughout all the process giving good advice and error correction when needed, my colleague Diego Samaniego for his invaluable tips working together in the lab and David Zurita, who always took care of me when I had problems regarding devices at the lab that were needed for the system.

References

[1] D. Novak and J. Capmany. Microwave Photonics combines two worlds. *Nature Photonics*, 1:319–330, 2007.

[2] B. Vidal, T. Nagatsuma, N.J. Gomes, and T.E. Darcie. Photonic Technologies for Millimeter- and Submillimeter-wave Signals. *Advances in Optical Technology*, 1:1–18, 2012.

[3] D. Wake, A. Nkansah, and N.J. Gomes. Radio over fiber link design for next generation wireless systems. *Journal of Lightwave Technology*, 28:2456–2464, 2010.

[4] M.A. Piqueras, T. Mengual, J. Blasco, M. Aamer, O. Navasquillo, and J.I. Ramirez. Optical harness (OHA) for future L-band radiometer. *International Conference on Space Optics - ICSO 2018*, 2:1–3, 2018.

[5] B. Vidal, D. Madrid, J.L. Corral, and J. Martí. Novel Photonic True-Time Delay Beamformer based on the Free Spectral Range Periodicity of Arrayed Waveguide Gratings and Fiber Dispersion. *IEEE Photonic Technology Letters*, 14:1614–1616, 2002.

[6] B. Vidal, J. Palaci, and J. Capmany. Reconfigurable Photonic Microwave Filter based on Four-Wave Mixing. *IEEE Photonics Journal*, 4:759–764, 2012.

[7] A. Bockelt, J. Palací, and B. Vidal. All-fiber Centralized Architecture for Parallel Terahertz Sensors. *IEEE Transactions on Terahertz Science and Technology*, 5:137–144, 2015.

[8] B. Vidal. Photonic Technique for the Measurement of Frequency and Power of Multiple Microwave Signals. *IEEE Transactions on Microwave Theory and Techniques*, 58:3103–3108, 2010.

[9] B. Vidal. Photonic millimeter-wave frequency multiplication based on cascaded four-wave mixing and polarization pulling. *Optics Letters*, 37:5055–5057, 2012.

[10] M. Abdin, W. Joel, D. Johnson, and T. Weller. A System and Technology Perspective on Future 5G mm-Wave Communication Systems. *IEEE*, 2017.

[11] Z. Xiao, Q. Yang, J. Huang, Z. Huang, W. Zhou, Y. Gao, R. Shu, and Z. He. Terahertz communication windows and their point-to-point transmission verification. *IEEE*, 57:7673–7680, 2018.

[12] L. Tao, Z. Dong, J. Yu, N. Chi, J. Zhang, X. Li, Y. Shao, and G. Chang. Experimental Demonstration of 48-Gb/s PDM-QPSK Radio-Over-Fiber System Over 40-ghz mm-Wave MIMO Wireless Transmission. *Journal of Lightwave Technology*, 24:2276–2279, 2012.

[13] J. Yao. Microwave Photonics. *IEEE*, 7:314–335, 2009.

[14] T. Nagatsuma, G. Ducournau, and C. Renaud. Advances in Terahertz Communications Accelerated by Photonics. *Nature Photonics*, 10:371–379, 2016.

[15] T. Nagatsuma. THz communication systems. *Optical Fiber Conference (OFC)*, 2017.

[16] S. Jia, X. Yu, H. Hu, J. Yu, P. Guan, F. Da Ros, M. Galili, T. Morioka, and L.K. Oxenløwe. THz photonic wireless links with 16-QAM modulation in the 375-450 ghz band. *Optics Express*, 24:23777–23783, 2016.

[17] X. Yu, S. Jia, H. Hu, M. Galili, T. Morioka, P. U. Jepsen, and L. K. Oxenløwe. 160 Gbit/s photonics wireless transmission in the 300-500 GHz band. *Optics Express*, 1:081301, 2016.

[18] X.Pang, S. Jia, O. Ozolins, X. Yu, H. Hu, L. Marcon, P. Guan, F. Da Ros, S. Popov, G. Jacobsen, M. Galili, T. Morioka, D. Zibar, and L.K. Oxenløwe. 260 Gbit/s Photonic-Wireless Link in the THz Band. *IEEE*, 2016.

[19] X. Li, J. Yu, K. Wang, W. Zhou, and J. Zhang. Photonic-aided 2x2 MIMO wireless terahertz-wave signal transmission system with optical polarization multiplexing. *Optics Express*, 25:33236–33242, 2017.

[20] J. Ma, R. Shrestha, L. Moeller, and D. Mittleman. Channel Performance for Indoor and Outdoor Terahertz Wireless Links. *APL Photonics*, 3:051601, 2018.

[21] S. Jia, X. Pang, O. Ozolins, X. Yu, H. Hu, J. Yu, P. Guan, F. Da Ros, S. Popov, G. Jacobsen, M. Galili, T. Morioka, D. Zibar, and L.K Oxenløwe. Photonic-aided 2x2 MIMO wireless terahertz-wave signal transmission system with optical polarization multiplexing. *IEEE*, 25:33236–33242, 2017.

[22] S. Jia, M. Lo, L. Zhang, O. Ozolins, A. Udalcovs, D. Kong, X. Pang, X. Yu, S. Xiao, S. Popov, J. Chen, G. Carpintero, T. Morioka, H. Hu, and L.K. Oxenløwe. Integrated Dual-DFB Laser for 408 GHz Carrier Generation Enabling 131 Gbit/s Wireless Transmission over 10.7 Meters. *OSA*, 2019.

[23] A. Hirata, T. Kosugi, H. Takahashi, J. Takeuchi, H. Togo, M. Yaita, N. Kukutsu, K. Aihara, K. Murata, Y. Sato, T. Nagatsuma, and Y. Kado. 120-GHz-Band Wireless Link Technologies for Outdoor 10-Gbit/s Data Transmission. *IEEE*, 60, 2012.

[24] X. Li, J. Yu, J. Zhang, Z. Dong, F. Li, and N. Chi. A 400G optical wireless integration delivery system. *OSA*, 21:188812–188819, 2013.

[25] S. Koenig, D. Lopez-Diaz, J. Antes, F. Boer, R. Hennenberger, A . Leuther, A. Tessman, R. Schmogrow, D. Hillerkuss, R. Palmer, T. Zwick, C. Koos, W. Freude, O. Amabacher, J. Leuthold, and I. Kallfass. Wireless Sub-THz communication system with high data rate. *Nature Photonics*, 7:977–981, 2013.

[26] T. Nagatsuma, S. Horiguchi, Y. Minamikata, Y. Yoshimizu, S. Hisatake, S. Kuwano, N. Yoshimoto, J. Terada, and H. Takahashi. Terahertz wireless communications based on photonics technologies. *OSA*, 21:188812–188819, 2013.

[27] H. Shams, M. Fice, K. Balakier, C. Renaud, F. van Dijk, and A. Seeds. Photonic generation for multichannel thz wireless communication. *OSA*, 22:23465–23472, 2014.

[28] G. Ducournau, P. Szriftgiser, A. Beck, D. Bacqet, F. Paravello, E. Peytavit, M. Zaknoune, T. Akalin, and J. Lampin. Ultrawide-Bandwidth Single-Channel 0.4 THz Wireless Link Combining Broadband Quasi-Optic Photomixer and Coherent Detection. *IEEE*, 4:328–332, 2014.

[29] A. Kanno, T. Kuri, I. Morohashi, I. Hosako, T. Kawanishi, Y. Yoshida, and K. Kitayama. Coherent terahertz wireless signal transmission using advanced optical fiber communication technology. *J. Infrared, Mil. and THz waves*, 36:180–197, 2015.

[30] G. Ducournau, K. Engenhardt, P. Szriftgiser, D. Bacqet, M. Zaknoune, R. Kassi, E. Lecomte, and J. Lampin. 32 Gbit/s QPSK transmission at 385 GHz using coherent fibre-optic technologies and thz double heterodyne detection. *IEEE*, 51:915–917, 2015.

[31] X. Yu, R. Asif, M. Piels, D. Zibar, M. Galili, T. Morioka, P. Jepsen, and L.K. Oxenløwe. 400-GHz Wireless Transmission of 60-Gb/s Nyquist-QPSK Signals using UTC-PD and Heterodyne Mixer. *IEEE*, 6:765–770, 2016.

[32] L. Moeller, J. Federici, and K. Su. 2.5 Gbit/s duobinary signalling with narrow bandwidth 0.625 terahertz source. *IET*, 47:856–858, 2011.

[33] J. Antes, S. König, A. Leuther, H. Massler, J. Leuthold, O. Ambacher, and I. Kallfass. 220 GHz wireless data transmission experiments up to 30 Gbit/s. *IEEE*, 2011.

[34] C. Wang, B. Lu, C. Lin, Q. Chen, L. Miao, X. Deng, and J. Zhang. 0.34-THz Wireless Link Based on High-Order Modulation for Future Wireless Local Area Network Applications. *IEEE*, 4:75 – 85, 2014.

[35] M. Fujishima, S. Amakawa, K. Takano, K. Katayama, and T. Yoshida. Tehrahertz CMOS Design for Low-Power and High-Speed Wireless Communication. *IEEE*, pages 1091–1104, 2015.

[36] I. Kallfass, F. Boes, T. Messinger, J. Antes, A. Inam, U. Lewark, A. Tessmann, and R. Hennenberger. 64 Gbit/s Transmission over 850 m Fixed Wireless Link at 240 GHz Carrier Frequency. *J. Infrared, Mil. and THz waves*, 36:221–233, 2015.

[37] I. Kallfass, I . Dan, S. Rey, P. Harati, J. Antes, S. Wagner Tessmann, M. Kuri, R. Weber, H. Massler, A. Leuther, T. Merkle, and T. Kürner. Towards MMIC-based 300GHz Indoor Wireless Communication Systems. *J. Infrared, Mil. and THz waves*, E98:1081–1090, 2015.

[38] C. Paoloni, S. Boppel, V. Krozer, R. Leticia, E. Limiti, F. Magne, M. Marilier, A. Ramírez, B. Vidal, T. Le, and R. Zimmerman. Sub-THz components for high capacity point to multipoint wireless. *44th International Conference on Infrared, Millimeter and Terahertz Waves (IRMMW-THz), Paris (France)*, pages 1–6, 2019.

[39] B.Vidal. Analytical model for hybrid amplitude and phase modulation in dispersive radio over fiber links. *Optics Communications*, 284:5138–5143, 2011.

[40] J. Zhang, N. Chi, J. Yu, J. Zhu, Y. Shao, B. Huang, and L. Tao. Generation of 113 Coherent and Frequency-lock Multicarriers Using Cascaded Phase Modulators and EDFA Loop for Tb/s Optical Communications. *IEEE*, 2011.

[41] M.A. Piqueras Ruipérez. *Línea de retardo óptica basada en AWG y fibra dispersiva*. B.s. thesis, U. Politècnica de Valencia, Valencia, 2003.

[42] J.M. Fuster Escuder. *Aplicaciones de moduladores electroópticos de intensidad*. PhD thesis, U. Politècnica de Valencia, Valencia, 1998.

[43] W. Loh. *The Physics of Phase-Noise Mitigation: Signal Generation and Filtering Using Microwave-Photonic Links*. PhD thesis, Massachusetts Institute of Technology, Cambridge, Massachusetts, 2013.

[44] T. Shao, H. Shams, P. M. Anandarajah, M. J. Fice, C. C. Renaud, F. van Dijk, A. J. Seeds, and L.P. Barry. Phase Noise Investigation of Multicarrier Sub-THz Wireless Transmission System Based on an Injection-Locked Gain-Switched Laser. *IEEE Transactions on Terahertz Science and Technology*, 5:590–597, 2015.

[45] T.Shao, M. Beltrán, R. Zhou, P. M. Anandarajah, R. Llorente, and L.P. Barry. 60 GHz Radio Over Fiber System Based on Gain-Switched Laser. *Journal of Lightwave Technology*, 32:3695–3703, 2014.

[46] A. Ferreira, T. Silveira, D. Fonseca, R. Ribeiro, and P.Monteiro. External modulator linearization techniques for high performance radio over fiber transmission systems. *IEEE*, 2009.

[47] G. Zhang, X. Zheng, S. Li, H. Zhang, and B. Zhou. Postcompensation for nonlinearity of Mach–Zehnder modulator in radio-over-fiber system based on second-order optical sideband processing. *Optics Letters*, 37:806–808, 2012.

[48] Charles H. Cox III. *Analog optical Links. Theory and practice.* Cambridge University Press, New York, 2004.

[49] Vincent J. Urick Jr, Jason D. Mckinney, and Keith J. Williams. *Fundamentals of microwave photonics.* Wiley, New Jersey, 2015.

[50] R. Shafik, Md. Rahman, A. Islam, and N. Ashraf. On The Error Vector Magnitude As A Performance Metric And Comparative Analysis. *IEEE*, 2006.

[51] R.Schmogrow, B. Nebendahl, M. Winter, A. Josten, D. Hillerkuss, S. Koenig, J. Meyer, M. Dreschmann, M. Huebner, C. Koos, J. Becker, W. Freude, and J. Leuthold. Error Vector Magnitude as a Performance Measure for Advanced Modulation Formats. *IEEE Photonics Technology Letters*, 24:61–63, 2012.

[52] A. J. Metcalf, V. Torres-Company, D. E. Leaird, and A. M. Weiner. High-Power Broadly Tunable Electrooptic Frequency Comb Generator. *IEEE*, 19, 2013.

[53] V. Torres-Company and A. M. Weiner. Optical frequency comb technology for ultra-broadband radio-frequency photonics. *Laser photonics reviews*, 8:368–393, 2014.

[54] T.Shao, E. Martin, P. M. Anandarajah, C. Browning, V. Vujicic, R. Llorente, and L.P. Barry. Chromatic Dispersion-Induced Optical Phase Decorrelation in a 60 GHz OFDM-RoF System. *IEEE Photonics Technology Letters*, 26:2016–2019, 2014.

A Component parameters

Device	Parameter	Value
Laser	RIN	-145 dB/Hz
	Wavelength	1550 nm
	Input power	13 dB
EDFA 1	Noise figure	10 dB @ 0 dBm input
	Gain	30 dB @ 0 dBm input
	Optical bandwidth	30 nm
EDFA 2	Noise figure	5.5 dB @ -3dBm input
	Gain	30 dB @ -30 dBm input
	Optical bandwidth	35 nm
PM	IL	3 dB
	Vπ	3.1 V @ 1 GHz
FBG	Bandwidth	0.2 nm
	IL	0.4 dB
	Reflectivity	90%
DP-MZM	IL	4.8 dB
	Vπ	4.81 V @ 1 GHz
UTC	$\mathfrak{R}$	0.26 A/W
	Electrical bandwidth	2.5 GHz
	ZL	50 Ω
	Dark current	40 nA
	Temperature	300K

Table 3: Parameters of the system devices.